Black: referee's comments red: authors' answers
First of all, we want to thank the referee 2 and 3 for the detailed analysis of our paper.
For the details, please look into the paper with keeping track of changes.

Anonymous Referee #2

General comments: This is an important and valuable data to assess temporal and spatial variations of CO_2 in North China. However, this data must be further discussed in order to support the main reasons of those CO_2 variations. Comparisons with other megacities will be a good approach to improve the discussions.
Thanks for your suggestions.

In the revised paper, we add the CO_2 measurements at five urban sites in USA with a similar latitude of BJ. All these five sites belong to the CO_2 Urban Synthesis and Analysis (CO2-USA) Data Synthesis Network (Feng et al., 2016). The site locations, elevations, inlet heights, and references are listed in Table 1. As the CO_2 measurements at these five sites do not cover the period between October 2018 and September 2019, we use the latest 1-year available CO_2 measurements.

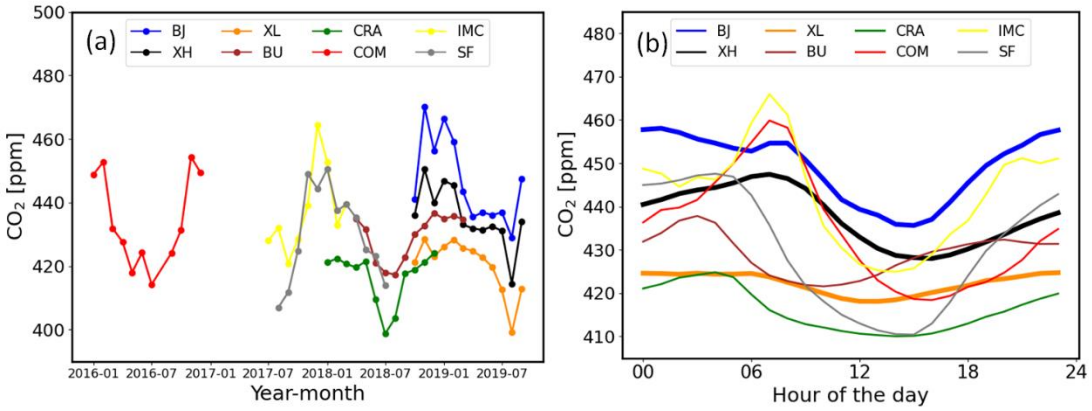

Figure 1. (a) Monthly means of CO_2 at BJ (L1), XH (L1), XL between October 2018 and September 2019, at BU, CRA, COM, IMC and SF during the latest 1 year and (b) the diurnal cycles of CO_2.

The monthly means and diurnal cycles of CO_2 at BJ (L1), XH (L1), XL, and 5 American urban sites are shown in Figure 1. It is found that the phases of the seasonal CO_2 cycles at BU, CRA, COM, IMC and SF are consistent with the observations at BJ (L1), XH (L1) and XL, with a high value in autumn-winter and a low value in summer. Among the five American sites, the highest CO_2 concentration is observed at IMC. The IMC site is inside a commercial zone and the CO_2 measurements over there are more strongly influenced by local emissions over there (Bares et al., 2019). The CO_2 concentration is also high at COM, because the Los Angeles megacity is one of the largest fossil fuel CO_2 emitters in the world (Matthäus et al., 2021). Figure 1 (a) shows that the CO_2 concentrations at COM and IMC are in the same level with the one at XH, but are less than the CO_2 concentration at BJ. The CO_2 concentrations at SF, BU and CRA are much lower as compared to BJ, because of lower anthropogenic emissions at these sites (McKain et al., 2015; Lauvaux et al., 2016; Shusterman et al., 2016).

Figure 1 (b) shows the diurnal variations of CO_2, with the amplitudes of 22.4, 19.4, 6.6, 16.3, 14.8, 41.5, 41.1 and 37.2 ppm at BJ (L1), XH (L1), XL, BU, CRA, COM, IMC and SF, respectively. The amplitudes of the diurnal variation at COM, IMC and SF are higher than that at BJ, although the yearly mean CO_2 levels at these sites are smaller than that at BJ. As the sampling heights at these sites and BJ are similar, the large amplitudes of the diurnal variation indicate that stronger variation in the local emissions and/or sinks exists at these three American sites as compared to BJ.

Table 1. Site characteristics of BJ, XH and XL in North China, BU, CRA, COM, IMC and SF in USA from the CO_2 Urban Synthesis and Analysis (CO2-USA) Data Synthesis Network.

Site Code	Site Name	Lat (°N)	Lon (°E)	Elevation (m a.s.l.)	Inlet Height (m a.g.l.)	City	Reference
BJ	Beijing	39.96	116.36	49	80/280	Beijing	Cheng et al., 2018
XH	Xianghe	39.75	116.96	30	60/80	Xianghe	Yang et al., 2020
XL	Xinglong	40.40	117.50	940	10	Xinglong	Yang et al.,2019
BU	Boston University	42.35	-71.10	4	29	Boston	Sargent et al., 2018 McKain et al., 2015
CRA	Crawfordsville	39.99	-86.74	264	76	Indianapolis	Lauvaux et al., 2016 Richardson et al., 2017
COM	Compton	33.87	-118.28	9	45	Los Angeles	Verhulst et al., 2017
IMC	Intermountain Medical Center	40.67	-111.89	1316	66	Salt Lake City	Mitchell et al., 2018 Bares et al., 2019
SF	SF Hospital Bldg 5	37.76	-122.41	23.9	52	San Francisco	Shusterman et al., 2016

Specific comments:

Section 2.2.2: Further description of calibration and data processing:

1) How CRDS stability was checked over time, before and after malfunctions?

Thanks for your suggestions. More information is added in the revised paper.

The intake system is connected to an 8-position valve, which is used to choose the air coming from the sample air, the target gas, or the calibration gas. The target and calibration gases are pressurized in 29.5 L treated aluminum alloy cylinders, which are scaled to the WMO X2007 standard by the China Meteorological Administration, Meteorological Observation Centre. The same calibration procedure is operated at these three sites: 1) 3-hours sample air; 2) 5-minutes calibration gas; 3) 3-hours sample air; 4) 5-minutes target gas. This process repeats every 6 hours and 10 minutes. Note that, the airs coming from two levels at XH and BJ are switched every 5 minutes during the 3-hours sample air period. As the remaining volume in the tubes needs time for flushing, the response of the analyzer turns to be stable about 1 minute after each switching. In order to reduce the uncertainty, we do not consider the first 3-minutes measurements after each switching.

The calibration gas is to calculate the calibration factor (*cf*),

$$cf = CO_{2,mcal}/CO_{2,cal} \quad (1)$$

where $CO_{2,mcal}$ is the CO_2 mole fraction measured by the Picarro analyzer from the calibration gas and $CO_{2,cal}$ is the standard CO_2 mole fraction of the calibration cylinder.

The target gas is used to check the precision and stability of the system. The T value are calculated as follows,

$$T = cf \times CO_{2,mtar} - CO_{2,tar} \quad (2)$$

where $CO_{2,tar}$ is the standard CO_2 mole fraction of the target gas cylinder, $CO_{2,mtar}$ is the CO_2 mole fraction measured by the Picarro analyzer from the target gas, cf is calculated from the CO_2 mole fraction measured by the Picarro analyzer from the calibration gas.

To keep the CRDS stable over time, only the periods with T value within ±0.1 ppm are selected. The measurement uncertainties of the Picarro instrument at the three sites are calculated as the standard deviation (std) of T, which are 0.01, 0.06, and 0.02 ppm at BJ, XH, and XL respectively.

2) Describe the steps used during data processing; what kind of filters were used?

Besides the calibration procedure, we also do auto and manual flagging of the raw data. In each 1-hour CO_2 measurement window, auto-flags are assigned when deviations from CO_2 mean are found larger than 2-times hourly CO_2 std. Furthermore, manual flags are assigned by technicians at each site according to the logbook to exclude no-valid data resulted from the inlet filter, pump, and extreme weather issues. In addition, as the CRDS measurement system records CO_2 and CH_4 simultaneously, the variations of these two gases are checked together to manually flag CO_2/CH_4 outliers.

All these information has been added in the revised version.

P5 – lines 101-102: Data filtering were not used to reduce uncertainties but to exclude no-valid data. Review this sentence.

Thanks for the suggestion. The sentence is rewritten now as: “Furthermore, manual flags are assigned by technicians at each site according to the logbook to exclude no-valid data resulted from the inlet filter, pump, and extreme weather issues.”

Results and discussion

Section 3.1 time series: Strategies/methods to selection of background mole fractions must be further presented and discussed in order to show low influence of anthropogenic sources.

Thanks for your suggestions.

In this study, we treat the CO_2 measurements at XL as the background of BJ and XH. In the revised paper, we use the CarbonTracker model, version CT-NRT.v2021-3 (Peters et al., 2005) to evaluate the influence of anthropogenic, biogenic, oceanic and fire sources at these three sites. The CarbonTracker is a data assimilation system developed by the National Oceanic and Atmospheric Administration (NOAA) to keep track of sources and sinks of atmospheric CO_2 around the world. Four tracers (biosphere, ocean, fire and fossil fuel) are treated separately to simulate atmospheric CO_2 mole fractions. Mustafa et al. (2020) evaluated the CarbonTracker model in Asia by comparing with satellite measurements, and they found that the CarbonTracker model captures the variation of CO_2 well. The model provides 3-hourly CO_2 data at 25 levels from surface to ~ 123 km, and the spatial resolution of the global CarbonTracker CO_2 simulation is 3°×2° (longitude x latitude). As BJ and XH are in the same model grid, we note the CO_2 simulations in the BJ/XH grid as BJ.

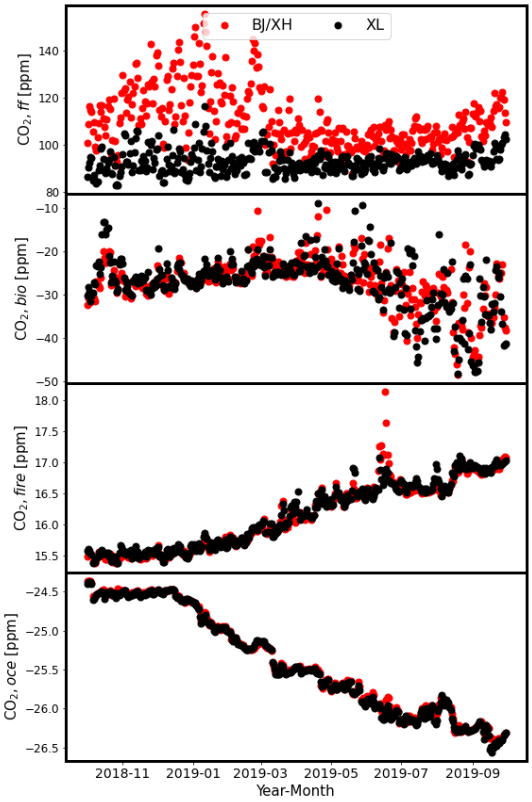

Figure 2. The time series of CO_2 simulations from fossil fuel ($CO_{2,ff}$), biosphere ($CO_{2,bio}$), fire ($CO_{2,fire}$) and ocean ($CO_{2,oce}$) modules at BJ/XH and XL.

Figure 2 shows the time series of CO_2 simulations from fossil fuel ($CO_{2,ff}$), biosphere ($CO_{2,bio}$), fire ($CO_{2,fire}$) and ocean ($CO_{2,oce}$) modules at BJ/XH and XL between October 2018 and September 2019. It is found that the fire and ocean CO_2 at BJ/XH and XL are close to each other throughout the whole year. The biogenic CO_2 at BJ/XH and XL have a similar level between October 2018 and June 2019, and become slightly different in summer 2019. However the difference in biogenic CO_2 is much less than that of the anthropogenic CO_2 differences. The variation of the fossil fuel CO_2 at XL is much less than that at BJ/XH. Therefore, by using the CO_2 measurements at XL as the background, we can significantly reduce the influence from fire, biosphere and ocean, and extract the signal of the anthropogenic CO_2 differences.

P7 - lines 138-144: Please add mean (std) concentrations related to higher and low CO_2 levels.
Done.
The mean Δ CO_2 at BJ and XH are 26.2±20.6 ppm and 15.2±13.6 ppm, respectively.

P7 – lines 149-150: Contribution of main sources (fossil fuel and heating) must be further discussed. Other sources as biomass burning from wildfires are important? If possible, trace gases/species would be used to identify activity of specific sources.
Thanks for the suggestions. More discussions are added now.

The Δ CO_2 has a maximum in winter and a minimum in summer at both BJ and XH. According to the CarbonTraker simulation, the high CO_2 concentrations at BJ and XH in winter are dominated

by the enhancement of fossil fuel. According to the Global Fire Assimilation System (GFAS) (https://www.ecmwf.int/en/forecasts/dataset/global-fire-assimilation-system) wildfire emissions, there is almost no biomass burning CO_2 emissions at BJ, XH and XL sites. The CarbonTraker model simulations confirm that fire CO_2 concentrations in this region are almost the same, and the simulated fire CO_2 at these sites are transported by the wildfire emissions at other places. What's more, the CarbonTraker model suggests that the fire CO_2 at these sites only take up a small proportion of the observed CO_2 (less than 5%).

P9 – lines 166-167: Discuss the reasons of higher amplitudes in BJ.
Thanks for the suggestions. More discussions are added now.

The amplitudes of the seasonal variation of CO_2 at BJ, XH and XL are 41.2 ppm, 36.1 ppm and 29.3 ppm, respectively. According to the CarbonTracker simulation, the CO_2 seasonal cycle in this region is mainly driven by the biogenic and anthropogenic CO_2. At XL, the anthropogenic CO_2 is almost constant through the whole year, while the biogenic CO_2 is low in summer and high in winter. For BJ/XH, apart from the similar biogenic CO_2 seasonal variation, the anthropogenic CO_2 is also high in winter and lower in summer. Therefore, combining the effect from the biosphere and human activities, the amplitude of CO_2 seasonal variation at BJ/XH is larger than that at XL. What's more, as the anthropogenic emission at BJ is much larger than that at XH, indicated by the EDGAR emission dataset, we thus observe the largest amplitude of the seasonal variation at BJ.

P9 – lines 216-217: References must be added to support the assumption.
Thanks for the suggestions. References are added now.

"The solar radiation is strongest at noon which leads to the largest photosynthesis removing CO_2 (Mohotti and Lawlor, 2002). The diurnal variation of CO_2 at daytime is then strongly affected by the plants in spring and summer, due to the large diurnal variation of the biogenic flux (high LAI) in these two seasons at XL (see Figure 3). However, in autumn and winter, the minimum of the CO_2 mole fraction occurs close to the maximum of the BLH, indicating that the diurnal variation is then dominated by the BLH (Newman et al., 2013), and the influence of the diurnal variation of the biogenic flux becomes less because of the low LAI in these two seasons."

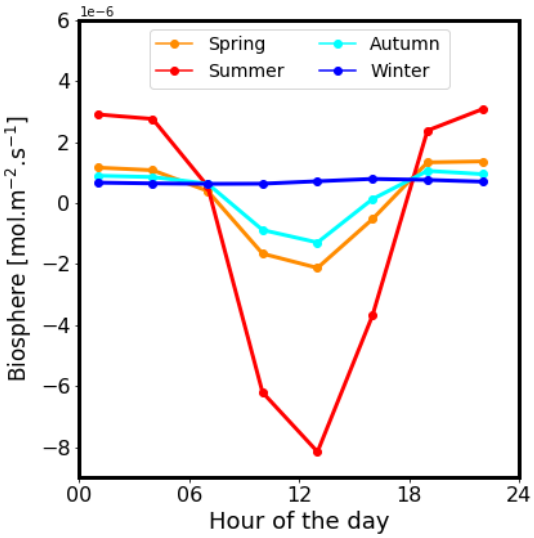

Figure 3. The daily variations of biological CO_2 surface flux in spring, summer, autumn and winter at XL estimated from CarbonTracker.

Section 3.5: Reasons to CO_2 mole fractions variations in L1 and L2 altitudes must be discussed.
Thanks for the suggestions, more discussions are added now.

Figure 10 in the ACPD shows the CO_2 hourly means observed at two levels at BJ and XH between October 2018 and September 2019. Note that, we select measurements when the hourly means are available at both levels.

At BJ, CO_2 mole fractions at L1 are generally higher than L2 as L1 is closer to near-ground human emissions. At BJ L1 (80 m a.g.l.), we can observe a peak in the early morning, which is corresponding to the transportation rush hour. The valley of CO_2 at BJ L1 occurs at 16:00-17:00 because of the maximum PBL resulting from the unstable atmosphere. After that, the atmosphere changes from unstable to stable during the night, leading to the CO_2 peak again. At BJ L2 (280 m a.g.l.), the diurnal variation of CO_2 generally follows that at L1. Note that the peak of the CO_2 at L2 occurs in the early morning later than that at L1 as the CO_2 at the ground level moved upward with the increase in convective PBL, with a large difference in winter and a small difference in summer. The CO_2 diurnal variations from two-layers Picarro measurements in 2018 and 2019 in our study are consistent with the seven open-path infrared gas analyzers (Model LI-7500A; at 8, 16, 47, 80, 140, 200 and 280 m a.g.l.) measurements between 2013 and 2016 at the same site (Cheng et al., 2018). In summer, the temperature is high due to a larger solar irradiance, the atmosphere becomes unstable quickly accelerating the uplifting of the PBL. In winter, the uplifting of the PBL is slow because of the stable atmosphere.

At XH, the CO_2 mole fractions at L1 and L2 are closer to each other as compared to the two-layers measurements at BJ, because the difference in the vertical distance of two layers at XH is only 20 m. Nevertheless, we can still observe that the peak of the CO_2 at L2 occurs in the early morning later than that at L1 as the CO_2 at the ground level moved upward with the increase in convective PBL, with a large difference in winter and a small difference in summer.

To compare the vertical distribution of CO_2 at BJ and XH, we calculate the CO_2 gradient (δCO_2 =

($CO_{2,L1}-CO_{2,L2}$)/($Alt_{L2}-Alt_{L1}$)) (Figure 10c). The diurnal variations of δCO_2 at BJ and XH have a similar pattern: close-zero during the day and positive at night. The maximum δCO_2 can reach to 0.6 ppm/m at XH in 2018 August and 0.2 ppm/m at BJ in 2018 November. The larger height difference at BJ (120 m) as compared to XH (20 m) may contribute to the smaller δCO_2.

Section 3.6: This section must be further assessed using different approaches. One of these strategies would be investigate seasonal differences during weekday-weekend.
P13 – line 255: Assumption of lowest anthropogenic emissions on Tuesday must be proven.
Thanks for your suggestions.

From the Figure 11 in the ACPD, we see a low CO_2 concentration as compared to other days. Therefore, we wrote "we find that the CO_2 mole fractions have a minimum on Tuesday at BJ and XH. It is indicated that the anthropogenic emission is lowest on Tuesday." The most three important CO_2 anthropogenic emissions in BJ are energy conversion, transport and industry (Yu et al., 2014, Crippa et al., 2020). Among these three, only transport emission has a strong day-to-day variation. According to the TomTom report (https://www.tomtom.com/en_gb/traffic-index/beijing-traffic/), we can recognize a decrease in the transport during the weekend but not in Tuesday. Therefore, in the revised version, we removed the original Figure 11, but add the plots to compare the CO_2 during weekdays and weekends.

Beijing traffic

WEEKLY TRAFFIC CONGESTION BY TIME OF DAY

What time was rush hour in Beijing?

	Sun	Mon	Tue	Wed	Thu	Fri	Sat
12:00 AM	0%	0%	0%	0%	1%	0%	1%
	0%	0%	0%	0%	0%	0%	0%
02:00 AM	0%	0%	0%	0%	0%	0%	0%
	0%	0%	0%	0%	0%	0%	0%
04:00 AM	0%	0%	0%	0%	0%	0%	0%
	0%	0%	0%	0%	0%	0%	0%
06:00 AM	1%	12%	8%	8%	8%	7%	0%
	3%	54%	46%	44%	44%	41%	5%
08:00 AM	8%	67%	59%	57%	56%	53%	13%
	13%	58%	52%	50%	49%	48%	20%
10:00 AM	16%	38%	37%	37%	36%	36%	26%
	15%	20%	22%	22%	22%	23%	26%
12:00 PM	12%	10%	12%	14%	13%	15%	19%
	11%	10%	12%	13%	13%	15%	14%
02:00 PM	18%	13%	16%	17%	17%	19%	19%
	21%	14%	17%	19%	18%	22%	21%
04:00 PM	23%	20%	22%	24%	24%	30%	23%
	29%	43%	46%	47%	47%	53%	30%
06:00 PM	29%	52%	54%	55%	55%	61%	31%
	22%	44%	45%	46%	45%	55%	23%
08:00 PM	13%	20%	20%	21%	21%	32%	12%
	8%	10%	11%	12%	12%	22%	7%
10:00 PM	4%	6%	7%	8%	8%	14%	4%
	1%	2%	3%	4%	3%	7%	1%

Figure 4. The traffic in Beijing within one week reported from TomTom.

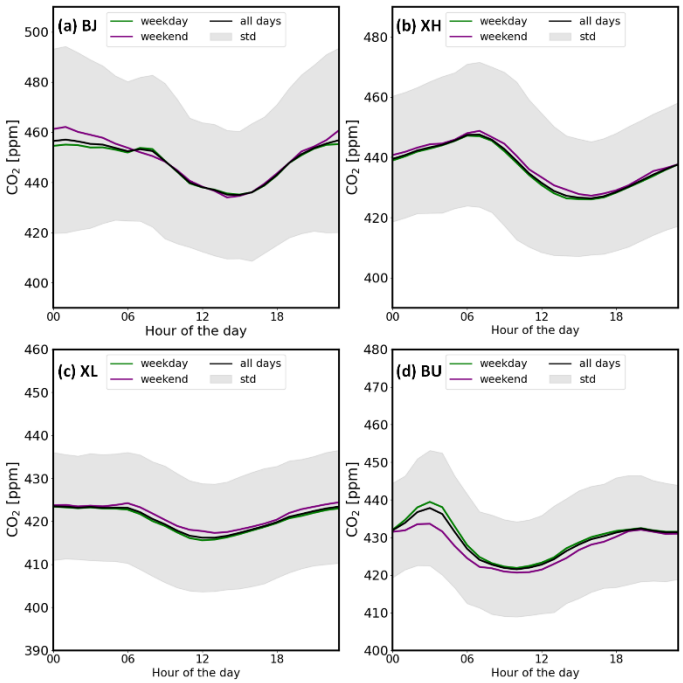

Figure 5. The average hourly means of CO_2 on weekday, weekend and all days at (a) BJ (L1), (b) XH (L1), (c) XL and (d) BU (Boston) between October 2018 and September 2019. The light gray shaded area represents one standard deviation from the mean for all days.

Figure 5 shows the average hourly means of CO_2 on weekday, weekend and all days at BJ (L1), XH (L1), XL between October 2018 and September 2019, and BU (Boston) between April 2018 and April 2019. At BJ (L1), the nighttime CO_2 measurements on weekend from 20 pm to 6 am next morning are generally ~5 ppm larger than those on weekday. XH (L1) and XL CO_2 measurements on weekend are ~2 ppm than those on weekday throughout the whole day respectively. On the contrary, BU CO_2 measurements on weekday are ~8 ppm larger than those on weekend between 4 and 6 am. The CO_2 differences on weekday and weekend at BU turn smaller after sunrise. The mean CO_2 at BJ (L1), XH (L1), XL and BU is 447.6, 436.2, 420.3 and 429.8 ppm respectively on weekday, and 449.2, 437.6, 421.4 and 427.5 ppm respectively on weekend. The weekday-weekend variations at BJ and XH are similar to that at Nanjing China (Gao et al., 2018), where CO_2 mole fractions are higher on weekends, but different from Boston USA, London UK and Tamil Nadu India, where the CO_2 mole fractions are higher on weekdays (Hernández-Paniagua et al., 2015; Kumar and Nagendra, 2015; Briber et al., 2013).

References

Bares, R., Mitchell, L., Fasoli, B., Bowling, D. R., Catharine, D., Garcia, M., Eng, B., Ehleringer, J., and Lin, J. C.: The Utah urban carbon dioxide (UUCON) and Uintah Basin greenhouse gas networks: instrumentation, data, and measurement uncertainty, Earth Syst. Sci. Data., 11, 1291–1308, https://doi.org/10.5194/essd-11-1291-2019, 2019.

Briber, B. M., Hutyra, L. R., Dunn, A. L., Raciti, S. M., and Munger, J. W.: Variations in

Atmospheric CO2 Mixing Ratios across a Boston, MA Urban to Rural Gradient, Land, 2, 304–327, https://doi.org/10.3390/land2030304, 2013.

Cheng, X. L., Liu, X. M., Liu, Y. J., and Hu, F.: Characteristics of CO2 Concentration and Flux in the Beijing Urban Area, J. Geophys. Res. Atmos., 123, 1785–1801, https://doi.org/10.1002/2017JD027409, 2018.

Crippa, M., Oreggioni, G., Guizzardi, D., Muntean, M., Schaaf, E., Vullo, E. L., Solazzo, E., Monforti-Ferrario, F., Olivier, J., and Vignati, E.: Fossil CO2 and GHG emissions of all world countries - 2019 Report, Publications Office of the European Union, Luxembourg, pp. ISBN 978–92–76–11 100–9, https://doi.org/10.2760/687800, 2019.

Feng, S., Lauvaux, T., Newman, S., Rao, P., Ahmadov, R., Deng, A., Díaz-Isaac, L. I., Duren, R. M., Fischer, M. L., Gerbig, C., Gurney, K. R., Huang, J., Jeong, S., Li, Z., Miller, C. E., O'Keeffe, D., Patarasuk, R., Sander, S. P., Song, Y., Wong, K. W., and Yung, Y. L.: Los Angeles megacity: a high-resolution land–atmosphere modelling system for urban CO2 emissions, Atmos. Chem. Phys., 16, 9019–9045, https://doi.org/10.5194/acp-16-9019-2016, https://acp.copernicus.org/articles/16/9019/2016/, 2016.

Gao, Y. Q., Lee, X. H., Liu, S. D., Hu, N., Wei, X., Hu, C., Liu, C., Zhang, Z., and Yang, Y. C.: Spatio-temporal variability of the near-surface CO2 concentration across an industrial-urban-rural transect, Nanjing, China, Sci. Total Environ., 631-632, 1192–1200, https://doi.org/10.1016/j.scitotenv.2018.03.126, 2018.

Hernández-Paniagua, I. Y., Lowry, D., Clemitshaw, K. C., Fisher, R. E., France, J. L., Lanoisellé, M., Ramonet, M., and Nisbet, E. G.: Diurnal, seasonal, and annual trends in atmospheric CO2 at southwest London during 2000–2012: Wind sector analysis and comparison with Mace Head, Ireland, Atmos. Environ., 105, 138 – 147, https://doi.org/10.1016/j.atmosenv.2015.01.021, 2015.

Kumar, M. K. and Nagendra, S. M. S.: Characteristics of ground level CO2 concentrations over contrasting land uses in a tropical urban environment, Atmos. Environ., 115, 286–294, https://doi.org/10.1016/j.atmosenv.2015.05.044, 2015.

Lauvaux, T., Miles, N. L., Deng, A., Richardson, S. J., Cambaliza, M. O., Davis, K. J., Gaudet, B., Gurney, K. R., Huang, J., O'Keefe, D., Song, Y., Karion, A., Oda, T., Patarasuk, R., Razlivanov, I., Sarmiento, D., Shepson, P., Sweeney, C., Turnbull, J., and Wu, K.: Highresolution atmospheric inversion of urban CO2 emissions during the dormant season of the Indianapolis Flux Experiment (INFLUX), J. Geophys. Res. Atmos., 121, 5213–5236, https://doi.org/10.1002/2015JD024473, 2016.

Matthäus, K., Annmarie, E., Dustin, R., Lin, J., Feng, S., Lei, R. X., Lauvaux, T., Oda, T., Roehl, C., Blavier, J. F., and Iraci, L.: Urbanfocused satellite CO2 observations from the Orbiting Carbon Observatory-3: A first look at the Los Angeles megacity, Remote Sens. Environ., 258, 112 314, https://doi.org/10.1016/j.rse.2021.112314, 2021.

Mitchell, L. E., Lin, J. C., Bowling, D. R., Pataki, D. E., Strong, C., Schauer, A. J., Bares, R., Bush, S. E., Stephens, B. B., Mendoza, D., Mallia, D., Holland, L., Gurney, K. R., and Ehleringer, J. R.: Long-term urban carbon dioxide observations reveal spatial and temporal dynamics related to urban characteristics and growth, Proc. Natl. Acad. Sci. U. S. A., 115, 2912–2917, https://doi.org/10.1073/pnas.1702393115, 2018.

Mustafa, F., Bu, L. B., Wang, Q., Ali, M. A., Bilal, M., Shahzaman, M., and Qiu, Z. F.: Multi-Year Comparison of CO2 Concentration from NOAA Carbon Tracker Reanalysis Model with Data from GOSAT and OCO-2 over Asia, Rem. Sens., 12, 2498, https://doi.org/10.3390/rs12152498, 2020.

Mohotti, A. J. and Lawlor, D. W.: Diurnal variation of photosynthesis and photoinhibition in tea: effects of irradiance and nitrogen supply during growth in the field, J. Exp. Bot. Copiar, pp. 313–322, 2002.

McKain, K., Down, A., Raciti, S. M., Budney, J., Hutyra, L. R., Floerchinger, C., Herndon, S. C., Nehrkorn, T., Zahniser, M. S., Jackson, R. B., Phillips, N., and Wofsy, S. C.: Methane emissions from natural gas infrastructure and use in the urban region of Boston, Massachusetts, Proc. Natl. Acad. Sci. U. S. A., 112, 1941–1946, https://doi.org/10.1073/pnas.1416261112, 2015.

Newman, S., Jeong, S., Fischer, M. L., Xu, X., Haman, C. L., Lefer, B., Alvarez, S., Rappenglueck, B., Kort, E. A., and Andrews, A. E.: Diurnal tracking of anthropogenic CO2 emissions in the Los Angeles basin megacity during spring 2010, Atmos. Chem. Phys., 13, 4359–4372, 2013.

Peters, W., Miller, J. B., Whitaker, J., Denning, A. S., Hirsch, A., Krol, M. C., Zupanski, D., Bruhwiler, L., and Tans, P. P.: An ensemble data assimilation system to estimate CO2 surface fluxes from atmospheric trace gas observations, J. Geophys. Res. Atmos., 110, https://doi.org/10.1029/2005JD006157, 2005.

Richardson, S. J. and Miles, N. L., Davis, K. J., Lauvaux, T., Martins, D. K., Turnbull, J. C., McKain, K., Sweeney, C., and L., M. O.: Tower measurement network of in-situ CO2, CH4, and CO in support of the Indianapolis FLUX (INFLUX) Experiment., Elementa: Science of the Anthropocene, 5, 59, https://doi.org/10.1525/elementa.140, 2017.

Sargent, M., Barrera, Y., Nehrkorn, T., Hutyra, L. R., Gately, C. K., Jones, T., McKain, K., Sweeney, C., Hegarty, J., Hardiman, B., Wang, J. A., and Wofsy, S. C.: Anthropogenic and biogenic CO2 fluxes in the Boston urban region, Proc. Natl. Acad. Sci. U. S. A., 115, 7491–7496, https://doi.org/10.1073/pnas.1803715115, 2018.

Shusterman, A. A., Teige, V. E., Turner, A. J., Newman, C., Kim, J., and Cohen, R. C.: The BErkeley Atmospheric CO2 Observation Network: 480 initial evaluation, Atmos. Chem. Phys., 16, 13 449–13, https://doi.org/10.5194/acp-16-13449-2016, 2016.

Verhulst, K. R., Karion, A., Kim, J., Salameh, P. K., Keeling, R. F., Newman, S., Miller, J., Sloop,

C., Pongetti, T., Rao, P., Wong, C., Hopkins, F. M., Yadav, V., Weiss, R. F., Duren, R. M., and Miller, C. E.: Carbon dioxide and methane measurements from the Los Angeles Megacity Carbon Project – Part 1: calibration, urban enhancements, and uncertainty estimates, Atmos. Chem. Phys., 17, 8313–8341, https://doi.org/10.5194/acp-17-8313-2017, 2017.

Yang, Y., Zhou, M., Langerock, B., Sha, M. K., Hermans, C., Wang, T., Ji, D., Vigouroux, C., Kumps, N., Wang, G., De Mazière, M., and Wang, P.: New ground-based Fourier-transform near-infrared solar absorption measurements of XCO2, XCH4 and XCO at Xianghe, China, Earth Syst. Sci. Data., 12, 1679–1696, https://doi.org/10.5194/essd-12-1679-2020, 2020.

Yang, Y., Wang, T., Wang, P. C., Zhou, M. Q., and Yao, B.: In-situ measurement of CO2 at the Xinglong regional background station over North China, Atmospheric and Oceanic Science Letters, 12, 385–391, https://doi.org/10.1080/16742834.2019.1644949, 2019.

Yu, H., Pan, SY., Tang, BJ. et al. Urban energy consumption and CO2 emissions in Beijing: current and future. Energy Efficiency 8, 527–543, https://doi.org/10.1007/s12053-014-9305-3, 2015.

Anonymous Referee #3

General comments: This is a carefully done study and the data is very valuable, but the preliminary data analysis and discussion have been done. What the main purpose of this study is? What's the main influencing mechanism of CO2? are there some differences with other big cites or megaregions?

Thanks for your suggestions.

The paper is aim to describe the spatial and temporal variations of CO_2 mole fractions in urban, suburban and rural areas of North China. And these measurements in and around cities are very useful for the climate and air pollution studies.

As is discussed in the paper, all the CO_2 variations at the three sites are influenced by the boundary layer height (BLH), photosynthesis and human activities. Generally, the increase of the BLH after sunrise and the photosynthetic uptake during the day make the CO_2 mole fraction decrease, but the BLH decreasing after sunset results into the accumulation of CO_2. However, at BJ, high CO_2 is more influenced by local human activities, and the CO_2 with the wind coming from the southwest is about ~21 ppm larger than those with the wind coming from the northwest during the day. At XL, besides the more significant impact of local photosynthesis, the wind from the cities in the south, such as Beijing and Tianjin, also makes CO_2 increase during the day.

In the revised paper, we add the CO_2 measurements at five urban sites in USA with a similar latitude of BJ. All these five sites belong to the CO_2 Urban Synthesis and Analysis (CO2-USA) Data Synthesis Network (Feng et al., 2016). The site locations, elevations, inlet heights, and references are listed in Table 1. As the CO_2 measurements at these five sites do not cover the period between October 2018 and September 2019, we use the latest 1-year available CO_2 measurements.

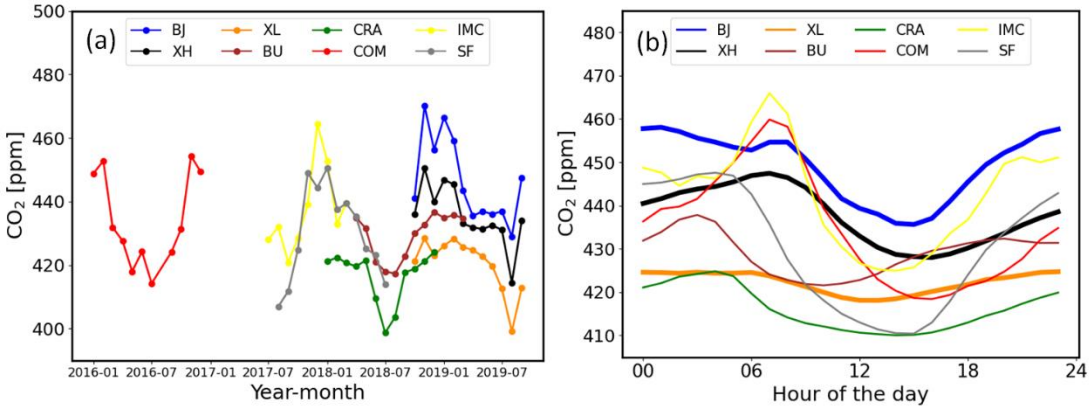

Figure 1. (a) Monthly means of CO_2 at BJ (L1), XH (L1), XL between October 2018 and September 2019, at BU, CRA, COM, IMC and SF during the latest 1 year and (b) the diurnal cycles of CO_2.

The monthly means and diurnal cycles of CO_2 at BJ (L1), XH (L1), XL, and 5 American urban sites are shown in Figure 1. It is found that the phases of the seasonal CO_2 cycles at BU, CRA, COM, IMC and SF are consistent with the observations at BJ (L1), XH (L1) and XL, with a high value in autumn-winter and a low value in summer. Among the five American sites, the highest CO_2 concentration is observed at IMC. The IMC site is inside a commercial zone and the CO_2

measurements over there are more strongly influenced by local emissions over there (Bares et al., 2019). The CO_2 concentration is also high at COM, because the Los Angeles megacity is one of the largest fossil fuel CO_2 emitters in the world (Matthäus et al., 2021). Figure 1 (a) shows that the CO_2 concentrations at COM and IMC are in the same level with the one at XH, but are less than the CO_2 concentration at BJ. The CO_2 concentrations at SF, BU and CRA are much lower as compared to BJ, because of lower anthropogenic emissions at these sites (McKain et al., 2015; Lauvaux et al., 2016; Shusterman et al., 2016).

Figure 1 (b) shows the diurnal variations of CO_2, with the amplitudes of 22.4, 19.4, 6.6, 16.3, 14.8, 41.5, 41.1 and 37.2 ppm at BJ (L1), XH (L1), XL, BU, CRA, COM, IMC and SF, respectively. The amplitudes of the diurnal variation at COM, IMC and SF are higher than that at BJ, although the yearly mean CO_2 levels at these sites are smaller than that at BJ. As the sampling heights at these sites and BJ are similar, the large amplitudes of the diurnal variation indicate that stronger variation in the local emissions and/or sinks exists at these three American sites as compared to BJ.

Table 1. Site characteristics of BJ, XH and XL in North China, BU, CRA, COM, IMC and SF in USA from the CO_2 Urban Synthesis and Analysis (CO2-USA) Data Synthesis Network.

Site Code	Site Name	Lat (°N)	Lon (°E)	Elevation (m a.s.l.)	Inlet Height (m a.g.l.)	City	Reference
BJ	Beijing	39.96	116.36	49	80/280	Beijing	Cheng et al., 2018
XH	Xianghe	39.75	116.96	30	60/80	Xianghe	Yang et al., 2020
XL	Xinglong	40.40	117.50	940	10	Xinglong	Yang et al.,2019
BU	Boston University	42.35	-71.10	4	29	Boston	Sargent et al., 2018 McKain et al., 2015
CRA	Crawfordsville	39.99	-86.74	264	76	Indianapolis	Lauvaux et al., 2016 Richardson et al., 2017
COM	Compton	33.87	-118.28	9	45	Los Angeles	Verhulst et al., 2017
IMC	Intermountain Medical Center	40.67	-111.89	1316	66	Salt Lake City	Mitchell et al., 2018 Bares et al., 2019
SF	SF Hospital Bldg 5	37.76	-122.41	23.9	52	San Francisco	Shusterman et al., 2016

Specific comments:

1. Please explain the data processing method and the proportion of valid data at the three sites.

Thanks for your suggestions. More information about the data processing method is added in the revised paper.

(1) Calibration

The intake system is connected to an 8-position valve, which is used to choose the air coming from the sample air, the target gas, or the calibration gas. The target and calibration gases are pressurized in 29.5 L treated aluminum alloy cylinders, which are scaled to the WMO X2007 standard by the China Meteorological Administration, Meteorological Observation Centre. The same calibration procedure is operated at these three sites: 1) 3-hours sample air; 2) 5-minutes calibration gas; 3) 3-hours sample air; 4) 5-minutes target gas. This process repeats every 6 hours and 10 minutes. Note

that, the airs coming from two levels at XH and BJ are switched every 5 minutes during the 3-hours sample air period. As the remaining volume in the tubes needs time for flushing, the response of the analyzer turns to be stable about 1 minute after each switching. In order to reduce the uncertainty, we do not consider the first 3-minutes measurements after each switching.

The calibration gas is to calculate the calibration factor (*cf*),

$$cf = CO_{2,mcal}/CO_{2,cal} \quad (1)$$

where $CO_{2,mcal}$ is the CO_2 mole fraction measured by the Picarro analyzer from the calibration gas and $CO_{2,cal}$ is the standard CO_2 mole fraction of the calibration cylinder.

The target gas is used to check the precision and stability of the system. The T value are calculated as follows,

$$T = cf \times CO_{2,mtar} - CO_{2,tar} \quad (2)$$

where $CO_{2,tar}$ is the standard CO_2 mole fraction of the target gas cylinder, $CO_{2,mtar}$ is the CO_2 mole fraction measured by the Picarro analyzer from the target gas, cf is calculated from the CO_2 mole fraction measured by the Picarro analyzer from the calibration gas.

To keep the CRDS stable over time, only the periods with T value within ±0.1 ppm are selected. The measurement uncertainties of the Picarro instrument at the three sites are calculated as the standard deviation (std) of T, which are 0.01, 0.06, and 0.02 ppm at BJ, XH, and XL respectively.

(2) Data Processing

Besides the calibration procedure, we also do auto and manual flagging of the raw data. In each 1-hour CO_2 measurement window, auto-flags are assigned when deviations from CO_2 mean are found larger than 2-times hourly CO_2 std. Furthermore, manual flags are assigned by technicians at each site according to the logbook to exclude no-valid data resulted from the inlet filter, pump, and extreme weather issues. In addition, as the CRDS measurement system records CO_2 and CH_4 simultaneously, the variations of these two gases are checked together to manually flag CO_2/CH_4 outliers.

The proportions of valid data are 98.5% and 99.1% at BJ L1 and L2, 99.3% and 99.1% at XH L1 and XH L2, 99.9% at XL.

All these information has been added in the revised version.

2. As CO_2 at XL is regarded as the background in this study, please explain whether there is a special data processing method for it, because the observational data at XL include not only the background information, but also local information about natural ecosystem and human activity, especially, the intake system of XL is on the roof.

Thanks for your suggestions.

In this study, we treat the CO_2 measurements at XL as the background of BJ and XH. In the revised paper, we use the CarbonTracker model, version CT-NRT.v2021-3 (Peters et al., 2005) to evaluate the influence of anthropogenic, biogenic, oceanic and fire sources at these three sites. The CarbonTracker is a data assimilation system developed by the National Oceanic and Atmospheric Administration (NOAA) to keep track of sources and sinks of atmospheric CO_2 around the world. Four tracers (biosphere, ocean, fire and fossil fuel) are treated separately to simulate atmospheric CO_2 mole fractions. Mustafa et al. (2020) evaluated the CarbonTracker model in Asia by comparing with satellite measurements, and they found that the CarbonTracker model captures the variation of

CO_2 well. The model provides 3-hourly CO_2 data at 25 levels from surface to ~ 123 km, and the spatial resolution of the global CarbonTracker CO_2 simulation is 3°×2° (longitude x latitude). As BJ and XH are in the same model grid, we note the CO_2 simulations in the BJ/XH grid as BJ.

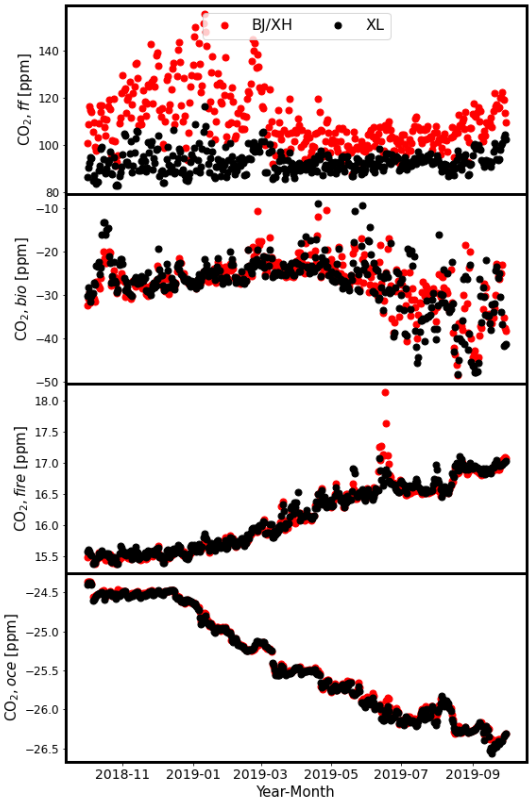

Figure 2. The time series of CO_2 simulations from fossil fuel ($CO_{2,ff}$), biosphere ($CO_{2,bio}$), fire ($CO_{2,fire}$) and ocean ($CO_{2,oce}$) modules at BJ/XH and XL.

Figure 2 shows the time series of CO_2 simulations from fossil fuel ($CO_{2,ff}$), biosphere ($CO_{2,bio}$), fire ($CO_{2,fire}$) and ocean ($CO_{2,oce}$) modules at BJ/XH and XL between October 2018 and September 2019. It is found that the fire and ocean CO_2 at BJ/XH and XL are close to each other throughout the whole year. The biogenic CO_2 at BJ/XH and XL have a similar level between October 2018 and June 2019, and become slightly different in summer 2019. However the difference in biogenic CO_2 is much less than that of the anthropogenic CO_2 differences. The variation of the fossil fuel CO_2 at XL is much less than that at BJ/XH. Therefore, by using the CO_2 measurements at XL as the background, we can significantly reduce the influence from fire, biosphere and ocean, and extract the signal of the anthropogenic CO_2 differences.

3. It is very pity that there are no meteorological parameters at XH. For the situation (2.1) and the meteorological field (2.3), it seems the air masses from BJ can be captured much more at XH because "the percentage of wind frequency in the north region is 34%, 36%, 50% and 60% respectively from spring to winter". And the air masses can be captured at XL only when the wind comes from SW.

Thanks for your the comment on this issue.

We are now devoting to fix the meteorology sensor at XH, which may provide more meteorological information in the future study.

References

Bares, R., Mitchell, L., Fasoli, B., Bowling, D. R., Catharine, D., Garcia, M., Eng, B., Ehleringer, J., and Lin, J. C.: The Utah urban carbon dioxide (UUCON) and Uintah Basin greenhouse gas networks: instrumentation, data, and measurement uncertainty, Earth Syst. Sci. Data., 11, 1291–1308, https://doi.org/10.5194/essd-11-1291-2019, 2019.

Cheng, X. L., Liu, X. M., Liu, Y. J., and Hu, F.: Characteristics of CO2 Concentration and Flux in the Beijing Urban Area, J. Geophys. Res. Atmos., 123, 1785–1801, https://doi.org/10.1002/2017JD027409, 2018.

Feng, S., Lauvaux, T., Newman, S., Rao, P., Ahmadov, R., Deng, A., Díaz-Isaac, L. I., Duren, R. M., Fischer, M. L., Gerbig, C., Gurney, K. R., Huang, J., Jeong, S., Li, Z., Miller, C. E., O'Keeffe, D., Patarasuk, R., Sander, S. P., Song, Y., Wong, K. W., and Yung, Y. L.: Los Angeles megacity: a high-resolution land–atmosphere modelling system for urban CO2 emissions, Atmos. Chem. Phys., 16, 9019–9045, https://doi.org/10.5194/acp-16-9019-2016, https://acp.copernicus.org/articles/16/9019/2016/, 2016.

Lauvaux, T., Miles, N. L., Deng, A., Richardson, S. J., Cambaliza, M. O., Davis, K. J., Gaudet, B., Gurney, K. R., Huang, J., O'Keefe, D., Song, Y., Karion, A., Oda, T., Patarasuk, R., Razlivanov, I., Sarmiento, D., Shepson, P., Sweeney, C., Turnbull, J., and Wu, K.: Highresolution atmospheric inversion of urban CO2 emissions during the dormant season of the Indianapolis Flux Experiment (INFLUX), J. Geophys. Res. Atmos., 121, 5213–5236, https://doi.org/10.1002/2015JD024473, 2016.

Matthäus, K., Annmarie, E., Dustin, R., Lin, J., Feng, S., Lei, R. X., Lauvaux, T., Oda, T., Roehl, C., Blavier, J. F., and Iraci, L.: Urbanfocused satellite CO2 observations from the Orbiting Carbon Observatory-3: A first look at the Los Angeles megacity, Remote Sens. Environ., 258, 112 314, https://doi.org/10.1016/j.rse.2021.112314, 2021.

McKain, K., Down, A., Raciti, S. M., Budney, J., Hutyra, L. R., Floerchinger, C., Herndon, S. C., Nehrkorn, T., Zahniser, M. S., Jackson, R. B., Phillips, N., and Wofsy, S. C.: Methane emissions from natural gas infrastructure and use in the urban region of Boston, Massachusetts, Proc. Natl. Acad. Sci. U. S. A., 112, 1941–1946, https://doi.org/10.1073/pnas.1416261112, 2015.

Mitchell, L. E., Lin, J. C., Bowling, D. R., Pataki, D. E., Strong, C., Schauer, A. J., Bares, R., Bush, S. E., Stephens, B. B., Mendoza, D., Mallia, D., Holland, L., Gurney, K. R., and Ehleringer, J. R.: Long-term urban carbon dioxide observations reveal spatial and temporal dynamics related to urban characteristics and growth, Proc. Natl. Acad. Sci. U. S. A., 115, 2912–2917, https://doi.org/10.1073/pnas.1702393115, 2018.

Mustafa, F., Bu, L. B., Wang, Q., Ali, M. A., Bilal, M., Shahzaman, M., and Qiu, Z. F.: Multi-Year Comparison of CO2 Concentration from NOAA Carbon Tracker Reanalysis Model with Data from GOSAT and OCO-2 over Asia, Rem. Sens., 12, 2498, https://doi.org/10.3390/rs12152498, 2020.

Peters, W., Miller, J. B., Whitaker, J., Denning, A. S., Hirsch, A., Krol, M. C., Zupanski, D., Bruhwiler, L., and Tans, P. P.: An ensemble data assimilation system to estimate CO2 surface fluxes from atmospheric trace gas observations, J. Geophys. Res. Atmos., 110, https://doi.org/10.1029/2005JD006157, 2005.

Richardson, S. J. and Miles, N. L., Davis, K. J., Lauvaux, T., Martins, D. K., Turnbull, J. C., McKain, K., Sweeney, C., and L., M. O.: Tower measurement network of in-situ CO2, CH4, and CO in support of the Indianapolis FLUX (INFLUX) Experiment., Elementa: Science of the Anthropocene, 5, 59, https://doi.org/10.1525/elementa.140, 2017.

Sargent, M., Barrera, Y., Nehrkorn, T., Hutyra, L. R., Gately, C. K., Jones, T., McKain, K., Sweeney, C., Hegarty, J., Hardiman, B., Wang, J. A., and Wofsy, S. C.: Anthropogenic and biogenic CO2 fluxes in the Boston urban region, Proc. Natl. Acad. Sci. U. S. A., 115, 7491–7496, https://doi.org/10.1073/pnas.1803715115, 2018.

Shusterman, A. A., Teige, V. E., Turner, A. J., Newman, C., Kim, J., and Cohen, R. C.: The BErkeley Atmospheric CO2 Observation Network: 480 initial evaluation, Atmos. Chem. Phys., 16, 13 449–13, https://doi.org/10.5194/acp-16-13449-2016, 2016.

Verhulst, K. R., Karion, A., Kim, J., Salameh, P. K., Keeling, R. F., Newman, S., Miller, J., Sloop, C., Pongetti, T., Rao, P., Wong, C., Hopkins, F. M., Yadav, V., Weiss, R. F., Duren, R. M., and Miller, C. E.: Carbon dioxide and methane measurements from the Los Angeles Megacity Carbon Project – Part 1: calibration, urban enhancements, and uncertainty estimates, Atmos. Chem. Phys., 17, 8313–8341, https://doi.org/10.5194/acp-17-8313-2017, 2017.

Yang, Y., Zhou, M., Langerock, B., Sha, M. K., Hermans, C., Wang, T., Ji, D., Vigouroux, C., Kumps, N., Wang, G., De Mazière, M., and Wang, P.: New ground-based Fourier-transform near-infrared solar absorption measurements of XCO2, XCH4 and XCO at Xianghe, China, Earth Syst. Sci. Data., 12, 1679–1696, https://doi.org/10.5194/essd-12-1679-2020, 2020.

Yang, Y., Wang, T., Wang, P. C., Zhou, M. Q., and Yao, B.: In-situ measurement of CO2 at the Xinglong regional background station over North China, Atmospheric and Oceanic Science Letters, 12, 385–391, https://doi.org/10.1080/16742834.2019.1644949, 2019.